A&A 436, 469–478 (2005)
DOI: 10.1051/0004-6361:20041664
© ESO 2005

Astronomy & Astrophysics

A Virgo high-resolution Hα kinematical survey

I. NGC 4438⋆

L. Chemin[1,2], V. Cayatte[3], C. Balkowski[2], P. Amram[4], C. Carignan[1], A. Boselli[5], C. Adami[5], M. Marcelin[4], O. Garrido[2,4], O. Hernandez[1,4], and J. Boulesteix[4]

[1] Département de Physique, Université de Montréal, CP 6128, Succ. Centre-ville, Montréal, Qc, H3C 3J7, Canada
e-mail: chemin@astro.umontreal.ca
[2] Observatoire de Paris, Section Meudon, GEPI, CNRS UMR 8111 & Université Paris 7, 5 Pl. Janssen, 92195 Meudon, France
[3] Observatoire de Paris, Section Meudon, LUTH, CNRS-UMR 8102 & Université Paris 7, 5 Pl. Janssen, 92195 Meudon, France
[4] Laboratoire d'Astrophysique de Marseille, 2 Pl. Le Verrier, 13248 Marseille, France
[5] Laboratoire d'Astrophysique de Marseille, Traverse du Siphon-Les trois Lucs, 13012 Marseille, France

Received 15 July 2004 / Accepted 28 February 2005

Abstract. New Hα emission-line observations of the Virgo cluster galaxy NGC 4438 are presented. Fabry-Perot interferometry data at an effective angular resolution of ∼2″ are used to map the kinematics of the ionized gas in the galaxy. For the first time we obtain a velocity field covering a large area in NGC 4438, much larger than that deduced from previous HI and CO maps. The kinematics of the extended, low surface brightness Hα filaments to the West of the galactic disk is discussed. We report on the discovery of a northern Hα structure which is clumpier than the other filaments. Evidence for multiple spectral components through the data-cube are presented in a nuclear shell and in the approaching half of the disk. The role of VCC 1040, a dwarf elliptical galaxy located to the South of NGC 4438, is presented to investigate the origin of a small-scale stellar tail of NGC 4438. It could be due to a minor tidal interaction between the two galaxies.

Key words. galaxies: clusters: individual: NGC 4438 – galaxies: interactions – galaxies: kinematics and dynamics

1. Introduction

The role of environmental effects is crucial for the evolution of galaxies. Galaxies undergo several different processes that directly affect their interstellar medium, modifying their morphology and perturbing their dynamics, particularly while crossing high density environments such as galaxy clusters. Well-known examples of such processes are tidal perturbations between galaxies (Moore et al. 1996; Gnedin 2003) and ram pressure stripping exerted by the hot intracluster medium (hereafter ICM, Gunn & Gott 1972).

The Virgo cluster galaxy NGC 4438 (VCC 1043) is a prototype of a disk interacting within a dense environment. Its main properties are listed in Table 1. It is one of the closest objects to the cluster core at only ∼1° in projection (or ∼280 kpc) from M 87 and ∼28′ (140 kpc) from M 86. Its morphology is the most perturbed among the Virgo galaxies, showing prominent stellar tails from North-East (NE) to South-West (SW) of the disk and a huge dust lane West of the disk (Fig. 1), molecular and neutral gas clouds displaced up to ∼1′ (4.7 kpc) West of the disk (Combes et al. 1988; Cayatte et al. 1990), very extended (up to ∼2′ or 9.4 kpc) ionized optical and X-ray emitting gas filaments (Kenney et al. 1995, hereafter referred to K95; Machacek et al. 2004) and an elongated region of 1.4 GHz continuum emission (Hummel et al. 1983). It is one of the most HI deficient disks in the cluster (Cayatte et al. 1990, 1994). Numerical simulations succeeded in explaining the NE and SW tidal tails formation by a past high-speed tidal encounter with NGC 4435, a northern companion (Combes et al. 1988). While a role for ram pressure stripping by the ICM was proposed to explain some observations (Kotanyi et al. 1983; Cayatte et al. 1990; Keel & Wehrle 1993), K95 speculated that the off-plane filamentary components could be regarded as consequences of an ISM-ISM interaction with NGC 4435.

In addition to this strongly disturbed large-scale morphology, Hα+[NII] *WFPC2-HST* imagery (Kenney & Yale 2002) and *Chandra* X-ray observations (Machacek et al. 2004) have revealed gaseous nuclear bipolar shells. The origin of these nuclear shells could be due to an AGN (Machacek et al. 2004).

Optical Fabry-Perot (FP) interferometry is quite appropriate to study the kinematics of NGC 4438 since the ionized gas is the only gaseous component covering both the inner disk regions as well as the outer ones. As part of a survey

⋆ Based on observations collected at the European Southern Observatory, Chile, program 69.B-0496, and at the Observatoire du Mont Mégantic, Québec, Canada.

Article published by EDP Sciences and available at http://www.edpsciences.org/aa or http://dx.doi.org/10.1051/0004-6361:20041664

Table 1. Basic properties of NGC 4438 (VCC 1043).

Right ascension (J2000)	$12^h\ 27^m\ 45.6^s$
Declination (J2000)	$+13°\ 00'\ 32''$
Type[1]	Sb (tides)
Nucleus[2]	LINER 1.9
Distance	16 Mpc
Linear scale	78 pc arcsec^{-1}
Heliocentric systemic velocity[3] v_{sys}	71 km s^{-1}
Inclination[4] i	87°
Disk position angle[3] PA	29°

[1] Morphological type from Binggeli et al. (1985).
[2] Ho et al. (1997).
[3] v_{sys} and PA from Kenney et al. (1995).
[4] i from LEDA.

Table 2. Observational setups.

Telescope	ESO 3.6 m	OmM 1.6 m
Observation date	2002, Apr., 6th	2004, Feb., 24th
Field of view	3.′6	13.′7
Data-cube size	$512 \times 512 \times 24$	$512 \times 512 \times 48$
(X, Y) pixel size	0.″42	1.″61
Interference order @ Hα	793	765
Free spectral range @ Hα (km s^{-1})	378	392
Channel width (km s^{-1})	15.75	8.16
Scanning wavelength (Å)	6564.3	6561.7
Interference filter central λ (Å)	6567.7	6565.0
Interference filter *FWHM* (Å)	12	30
Exposure time (s)	9360	14 400
Average seeing	0.″8	2.″5

dedicated to the study of the kinematics of Virgo Cluster galaxies (Chemin et al. 2004; Chemin et al. in preparation), FP interferometry observations of the Hα emission-line in NGC 4438 are used to map its complete kinematics for the first time. Section 2 presents the high resolution velocity field of the galaxy, which reveals the kinematics in the disk, in the nuclear shells and along the external filaments. In Sect. 3 the kinematics of the filaments as well as the role of ram pressure stripping in their evolution are discussed. Section 3 also proposes that a minor interaction with the dwarf elliptical galaxy companion VCC 1040 could be at the origin of morphological disturbances observed in the southern region of NGC 4438.

To be consistent with K95, a distance to the Virgo cluster of 16 Mpc is adopted throughout the article.

2. Observation and results

2.1. Data acquisition and reduction

One set of observations of NGC 4438 was performed in April 2002 at the 3.6 m European Southern Observatory telescope equipped with a focal reducer, a scanning FP interferometer and the photon counting camera FaNTOmM[1] (Gach et al. 2002). Table 2 describes the characteristics of the observations.

A FaNTOmM Hα emission-line observation obtained at the 1.6 m Observatoire du Mont Mégantic (OmM) Télescope was also used to map a large field of view around NGC 4435 and NGC 4438 (see Table 2). The observation is used to search for emission-lines outside the disk in the large-scale tails of NGC 4438. Although the OmM data-cube has low signal-to-noise ratio, the detection of ionized gas was successful in the disk and the brightest parts of the filaments, as well as at three locations represented by white squares in Fig. 1 (see also Table 3). Only the spectra at these three locations are presented for this observation (see Sect. 2.2).

[1] FaNTOmM stands for Fabry-Perot de Nouvelle Technologie de l'Observatoire du Mont Mégantic. See http://www.astro.umontreal.ca/fantomm for more details.

2.2. Hα Fabry-Perot emission-line and velocity maps

The basic pre-processing data reduction steps of raw FP data-cubes in order to obtain a calibrated data-cube have been described elsewhere (see e.g. Chemin et al. 2003). Once calibrated, the integrated emission of the galaxy corresponds to the sum of the signal of all channels above a continuum threshold. The threshold is chosen so that 15% of all the channels are under the continuum level, and the remaining 85% channels are consequently due to the Hα emission-line. We call this emission the total integrated emission. The pixel velocity corresponds to the barycentre of the emission-line. The case of a peculiar region for which some of its pixels exhibit two lines is described below. For these pixels, the velocity is not unique and a specific treatment must be done (see "Southern disk-Filament F4 region" paragraph).

Figures 1b and 2 present the total integrated Hα emission-line and the velocity field of NGC 4438 obtained using a data-cube appropriately smoothed to effective resolutions between 1.″26 and 2.″52 (corresponding to 3 and 6 pixels *FWHM*) in order to increase the signal-to-noise ratio in the field-of-view. Our Hα map is in good agreement with known deep Hα imagery (K95; Kenney & Yale 2002; Gavazzi et al. 2003). The Hα velocity field is in good agreement with the few long-slit measurements (K95) where both studies coincide. The most striking feature is the filamentary morphology extending West and South up to 2.′1 (or 9.8 kpc) from the nucleus and on which are superposed a few brighter clumps, probably HII regions. Some of these structures have already been described (K95; but see also Keel & Werhle 1993) and similar names as in K95 for the filaments will be used hereafter, as shown in the bottom-left corner of Fig. 1b. In the following, the kinematics of the different components of the galaxy are described: disk, nuclear shells, filaments and new found structures.

Disk. In the disk, the gas emission is dominated by few HII regions South and North from the nucleus and by a nuclear shell (see next paragraph). No attempt to derive an optical rotation curve was undertaken due to a highly inclined disk, obscured by dust lanes, that would cause large uncertainties in the circular velocities. The average minimum

Article published by EDP Sciences and available at http://www.edpsciences.org/aa or http://dx.doi.org/10.1051/0004-6361:20041664

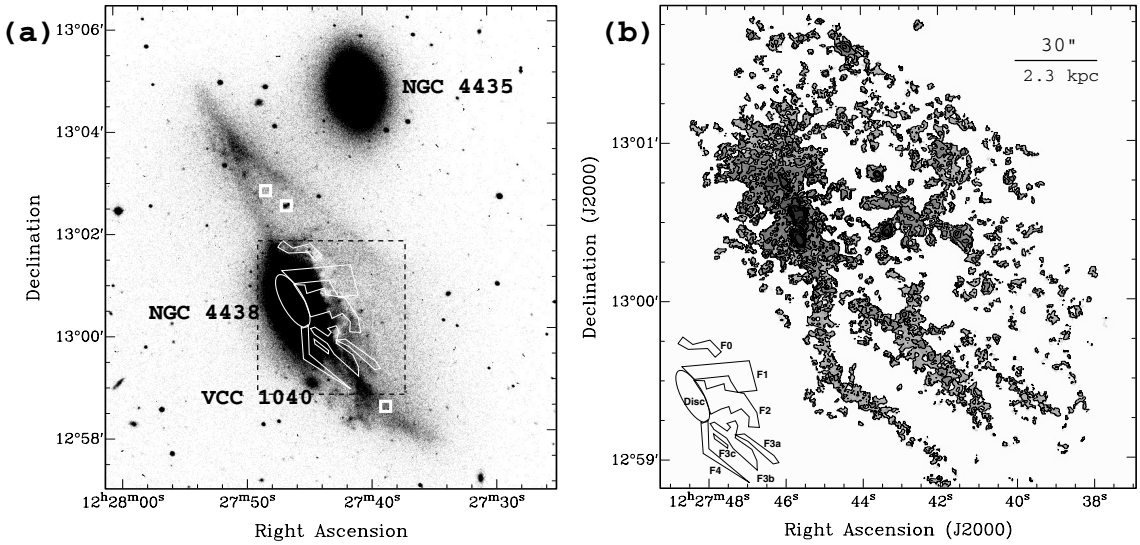


Fig. 1. a) A view of NGC 4435, NGC 4438 and VCC 1040. The optical map is a *B*-band image taken from the GoldMine database (Gavazzi et al. 2003). Contours display the approximate coverage of the total Hα emission. White squares correspond to the positions of selected spectra from the Mégantic FP observation (see Sect. 2.2, Table 3 and Fig. 6). The coordinates are in J2000. Notice the large dust layer on which the Hα emission superposes to the North and West of the disk of NGC 4438. A dashed box corresponds to the field of view seen in the right panel. **b)** Contours and grey-scale (displayed using a logarithmic stretch) map of the total integrated Hα emission. The first contour is at a higher intensity than the minimum level of the grey-scale image. The bottom-left, reduced-scale cartoon indicates the nomenclature used for the filaments.

Table 3. (*Top*) position-Velocity slice parameters along the major axis and Filament 4 from the ESO FP-observation. (*Bottom*) position of selected spectra in the OmM FP-observation.

ESO:		
Slice	**Centre coordinates (J2000)**	PA (°)
Major axis	$12^h27^m45\overset{s}{.}698$ +13°00′31.″38	29
Filament 4	$12^h27^m44\overset{s}{.}997$ +12°59′49.″57	180
OmM:		
Spectra	**Centre coordinates (J2000)**	**Velocity (km s^{-1})**
South (a)	$12^h27^m38\overset{s}{.}887$ +12°58′32.″73	–35
North (b)	$12^h27^m46\overset{s}{.}410$ +13°02′29.″27	–60
North (c)	$12^h27^m48\overset{s}{.}000$ +13°02′45.″00	–200

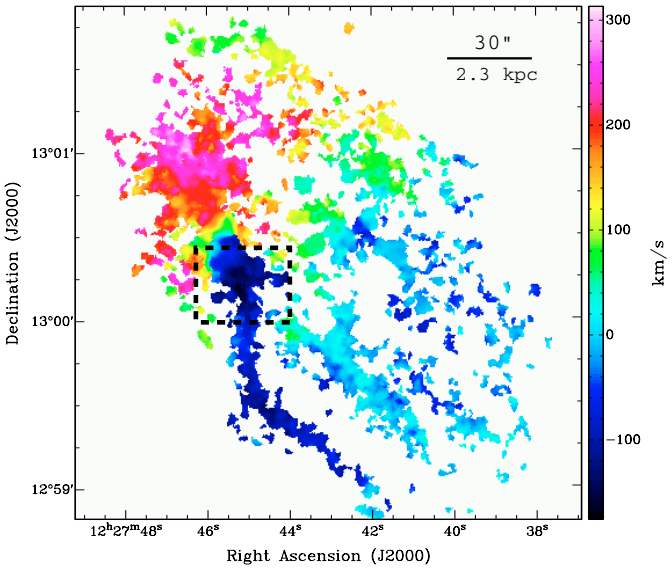


Fig. 2. Hα velocity field of NGC 4438. Radial velocities are respect to the heliocentric rest-frame. A dashed box corresponds to a region where two velocity components are detected in *some* of its pixels (see Sect. 2.2, paragraph "Southern disk-Filament F4 region"). The most blue-shifted velocity values are shown for these pixels. The location of these pixels is shown in Fig. 4a and their most red-shifted velocity values in Fig. 4b.

velocities are down to −150 km s^{-1} in the southern approaching half of the disk. Our results are consistent with the CO observations which show an inner molecular disk with velocities lower than −100 km s^{-1} (see Figs. 10 and 12 of K95, see also discussion in K95 about the Combes et al. observations).

Figure 3 represents the position-velocity diagram along the major axis of the galaxy (PA = 29°) and shows a classical rotating disk. The *kpvslice* task of the KARMA package (Gooch 1995) was used to make the position-velocity diagram. The pseudo-slit width is between 3 and 4 pixels (i.e. between 1.″3 and 1.″7) with a pixel weighting inversely proportional to the distance of the slice. For clarity reasons, a red solid line, which represents the velocity field values (Fig. 2), is drawn to follow the main interference order since more than one order is shown here. Lines are broader in the centre than in any other regions of the major axis.

Nuclear shells. Kenney & Yale (2002) found evidence for a bipolar nuclear shell in NGC 4438 from Hα+[NII] *WFPC2-HST* images. The NW and SE shells are intrinsically asymmetric in luminosity and length, in both optical and X-ray emission-lines and radio continuum (Kenney & Yale 2002;

Article published by EDP Sciences and available at http://www.edpsciences.org/aa or http://dx.doi.org/10.1051/0004-6361:20041664

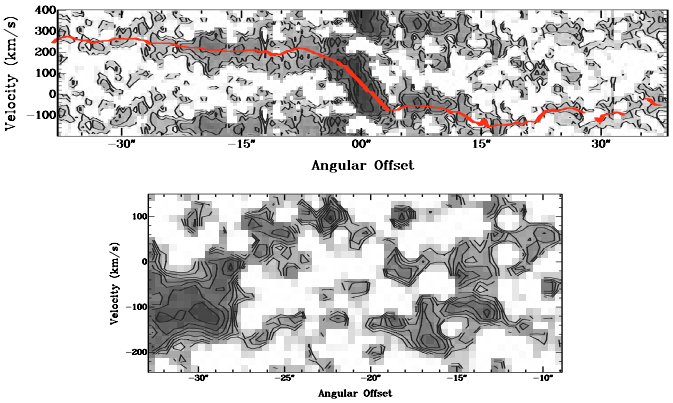


Fig. 3. Hα Position-velocity diagrams through different regions of the continuum-free data-cube. *Top*: along the major axis of the disk (PA = 29°). *Bottom*: along the Filament F4 (PA = 180°). A logarithmic grey-scale and contoured stretch is used for the Hα emission-line. A red solid line corresponds to the velocity field values (Fig. 2). The centre and orientation of the slices are listed in Table 3. The effective angular resolution of the data-cube used for the diagrams is 0.″84 (or 2 pixels *FWHM*).

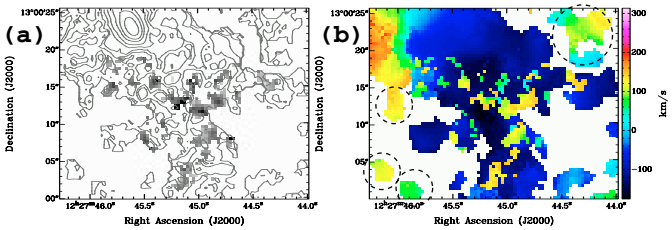


Fig. 4. Integrated emission **a)** and velocities **b)** of the most redshifted line for peculiar pixels in the dashed box region of Fig. 2 (see Sect. 2.2, paragraph "Southern disk-Filament F4 region" for details). **a)** The grey-scale pixels display the emission integrated under the most red-shifted emission line of these peculiar pixels and contours display the total integrated emission of the galaxy (already seen in Fig. 1b). **b)** Same velocity field as in Fig. 2 but this time showing the red-shifted velocity component for the peculiar pixels. Notice that these redshifted lines have velocities in contrast with that of the approaching half of the disk but in agreement with those of structures outside the disk and Filament F4 (encircled by dashed lines).

Machacek et al. 2004). Using an emission-line velocity dispersion measurement along the western edge of the NW shell, Kenney & Yale (2002) claimed that the shells are caused by a nuclear outflow in NGC 4438. Figure 1b shows that the NW shell is one of the brightest structure that is observed in the disk (RA ∼ $12^h27^m45.7^s$, Dec ∼ +13°00′33″) while the SE shell is indeed fainter (RA ∼ $12^h27^m46.5^s$, Dec ∼ +13°00′26″). Figure 2 shows that most of the gas motions in the SE shell is at $v_{obs} \sim 75 \pm 5$ km s^{-1}, which is close to the systemic velocity (71 km s^{-1}). At the tip of the shell, the velocities reach ∼115 km s^{-1}.

In Fig. 5, we focus on the NW shell kinematics. The shell has radial velocities increasing from ∼−60 km s^{-1} to ∼140 km s^{-1} (from SW to NE of the shell, respectively). We use here the high resolution Hα + [NII] *WFPC2-HST* images (Kenney & Yale 2002) taken from the *HST* archive and reduced as explained in Sect. 3.3. The velocities are close to the systemic velocity, principally along the apparent semi-major axis of the shell. As seen in spectra extracted from the *full angular resolution* data-cube and selected at different positions along the shell (right-panel diagrams of Fig. 5), the profiles are relatively wide in the shell. The restricted free spectral range of 380 km s^{-1} of the ESO-FP observation does not allow us to derive the velocity dispersions because the bases of the profiles are missing. The spectra show several velocity components. The major component in each spectrum is at a velocity given by the velocity field, close to the systemic velocity of the galaxy of ∼70 km s^{-1}. A redshifted (blue-shifted, respectively) component is detected at velocities up to ∼150 km s^{-1} (down to ∼50 km s^{-1}) relative to the systemic velocity. The blue-shifted component is detected in diagrams 1 to 3, but hardly in diagram 4. The reader should be aware that these additional components are known ±380 km s^{-1}, i.e. the ESO interfringe, because there is no direct way to determine the interference order at which they are emitting. Determining their true velocity would need larger spectral band observations than ours. Line splittings in nuclear shells often indicate an expanding bubble (Veilleux et al. 1994). This is here the first direct evidence that the shell is expanding. An accurate determination of the intrinsic outflow velocity and velocity dispersion would require a coupled kinematical and geometrical model of the shell (see e.g. Veilleux et al. 1994, for NGC 3079), which is beyond the scope of the article.

Filament F0. This northern filament was not previously described in K95 although present in their data. It is located at 65″ (5.1 kpc projected) North from the nucleus and is mostly traced by a string of Hα knots (probably HII regions) embedded in faint diffuse gas, running nearly parallel to the EW direction. Its morphology thus differs from that of the other filaments, which are mostly only diffuse. It has a length of 45″ (3.5 kpc) although it could be longer toward the SW and connected to Filament F1. Compared with a *B*-band image of the galaxy (Fig. 1), F0 exactly superposes on the northernmost part of the large western dust layer. Its velocities (∼80 km s^{-1}) are of the same order as the systemic velocity of NGC 4438 but admit a maximum of ∼110 km s^{-1} at its western tip – the HII clump at RA = $12^h27^m44.4^s$, Dec = +13°01′36″. The velocity of this latter clump is consistent with that of a HI counterpart at 120 km s^{-1} (Cayatte et al. 1990) as well as the one obtained with the long-slit observation (K95, their PA = 0° slit). A comparison of our Hα map with the *Chandra* X-ray image (Machacek et al. 2004) shows that F0 has no X-ray emission counterpart. Its evolution appears slightly different from that of the other filaments.

Filament F1. A velocity gradient is observed along part of the filament over a distance of 20″ (1.6 kpc) from 250 km s^{-1} down to about the systemic velocity of 71 km s^{-1} (from East to West respectively). One may notice that the western tip of F1 actually presents two regions with distinct velocities: a northern part at v_{obs} ∼ 130 km s^{-1} (RA ∼ $12^h27^m41.6^s$, Dec ∼ +13°01′10″) and a southern one at the systemic velocity. In fact, this northern part has a velocity comparable with that of the western extremity of F0 (within 20 km s^{-1}) and could be a genuine extension of F0. Combes et al. (1988) reported

Article published by EDP Sciences and available at http://www.edpsciences.org/aa or http://dx.doi.org/10.1051/0004-6361:20041664

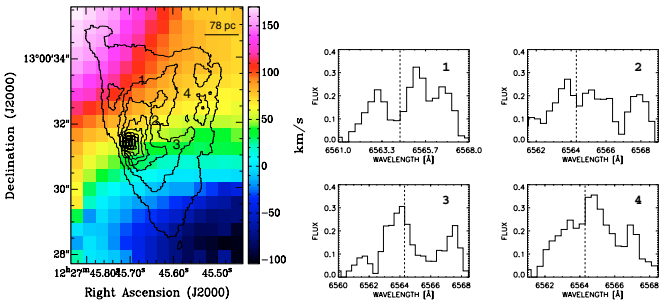


Fig. 5. Hα + [NII] *WFPC2-HST* contours of the NW nuclear shell (Kenney & Yale 2002) superposed on the corresponding Hα FP coloured velocity field. The spatial resolution of the Hα + [NII] HST image is 0.″1. The 78 pc segment corresponds to 1″ (D = 16 Mpc). Numbers 1 to 4 refer to the location of selected ESO-FP normalized continuum-free spectra along the shell (right panels). The flux unit of the spectra is arbitrary. The dashed lines indicate the systemic velocity of the galaxy.

wide CO-line profiles at a velocity of ∼85 km s^{-1} in the molecular cloud located at 1′ (4.7 kpc) NW from the nucleus. Taking into account the resolution of 23″ for the CO observations, it is probable that these two regions at significantly different velocities could not be resolved by the *IRAM* beam and thus artificially enlarged the CO emission-lines. These latter are then nearly centered at the velocity of the highest surface brightness component.

Filament F2. This filament also presents a velocity gradient, with velocities between ∼−15 km s^{-1} at its western tip and ∼200 km s^{-1} at the apparent connection with the disk. Compared with the largest neutral hydrogen concentration detected in the *VLA* observations (Cayatte et al. 1990), the Hα and HI velocities are very similar for the regions of overlap (60−80 km s^{-1}).

Filament F3. It is composed of three distinct, nearly parallel substructures F3a, F3b and F3c. F3b represents the main body of F3 and exhibits an average velocity of $\overline{v}_{\rm obs}$ ∼ 20 km s^{-1} occurring in its brightest parts, although lower velocities down to ∼−30 km s^{-1} are also observed along it, as well as higher ones (up to ∼70 km s^{-1}) at its eastern tip, close to F4. F3b actually presents wide profiles (up to 165 km s^{-1} *FWHM*, corrected for the instrumental Airy profile) which could be due to turbulent motions.

F3a has negative velocities (∼−25 km s^{-1}) to its NE side and null velocities (on average) on the other side. A new, short filament (F3c) is detected (∼15″, 1.2 kpc), barely seen and not discussed in K95. It appears to be linked to F3b by a ∼5″ (400 pc) ionized gas structure. F3c appears to be an extension of a bright warped stellar structure (see Fig. 7a) and mostly shows velocities of −20 km s^{-1}, but with a drop down to −80 km s^{-1}.

Filament F4. F4 appears to be the longest filament with a projected length of at least 1.′5 (7 kpc). Its first part originates in the southernmost side of the disk and is along the NS direction, running parallel but clearly offset from a stellar tidal tail (see Sect. 3.3 and Fig. 7a). Its second part is directed along the NE-SW direction and is almost parallel to F3.

F4 is the most blue-shifted filament w.r.t. the systemic velocity, presenting an average and nearly constant velocity of $\overline{v}_{\rm obs}$ ∼ −85 km s^{-1}. F4 may contribute to part of the kinematics in the southernmost parts of the disk but it is obviously less blue-shifted than further inside in the disk, where velocities down to −150 km s^{-1} are observed. It also exhibits a velocity drop (down to ∼−135 km s^{-1}) occurring in its bending region. Ionised gas at $\overline{v}_{\rm obs}$ ∼ −85 km s^{-1} is also observed close to the bending region but outside F4. The clump at the tip of F4 is at ∼−5 km s^{-1} and therefore appears kinematically independent from the whole filament.

Southern disk-Filament F4 region. The dashed box of Fig. 2 corresponds to a particular region, where F4 appears to meet the SW half of the disk. Some of its pixels exhibit two emission lines (Fig. 3). For those pixels, a barycentre computed over the whole profile, as done for all other pixels of the field-of-view that have only one spectral line, would give incorrect velocities due to the presence of the two competing lines. Two velocities need to be computed for them. A blue-shifted component has a velocity comparable with that of neighbouring pixels that show only one spectral component (<−100 km s^{-1}). It allows to follow a kinematic continuity in the SW approaching half of the disk. Its pixels are thus shown on the velocity map of Fig. 2. Figure 4 shows the pixels of the second, redshifted component (up to ∼100 km s^{-1}). A discontinuity is clearly seen with respect to the surrounding pixels showing only one emission line. Its kinematics is hard to reconcile with the rotating, approaching, blue-shifted pattern of the SW half of the disk and of Filament F4. It does not suggest that the emission comes from the disk or Filament F4, unlike the blue-shifted line. Its velocity is in better agreement with that of diffuse Hα structures outside the disk and F4 (see circles in Fig. 4). The pixels seem to connect these latter different redshifted structures, as if all the redshifted gas would belong to a same morphological structure. This latter could be an extension of Filament F2 to the East. The amplitude of the most redshifted line tends to be brighter than the blue-shifted one. However the transmission curve of the narrow interference filter may bias this claim (the filter transmission being higher in this part of the spectral range than in its blue part) so that it is hard to discriminate which component really dominates the total integrated emission. The integrated intensity map of the redshifted line is represented in grey-scale in Fig. 4, with contours showing the total Hα intensity. This local map should only be used to locate the peculiar pixels. Further observations would be needed to confirm our new finding and to accurately map the intensity of the most redshifted component.

Evidence for new structures. An isolated clump is detected West of F0 (RA = $12^{\rm h}27^{\rm m}42.5^{\rm s}$, Dec = +13°01′44″) with a radial velocity of 145 ± 5 km s^{-1}. It is barely seen in the Hα image of Kenney & Yale (2002) and no other molecular gas or HI counterparts have been observed at this location. The Hα image of Kenney & Yale (2002) also shows two other isolated knots located at 60″ and 65″ NE from the nucleus and close to the eastern edge of their field of view. These knots do not present Hα emission in the FP data-cube but typical continuum profiles and thus they could be foreground stars or more distant ojects.

Article published by EDP Sciences and available at http://www.edpsciences.org/aa or http://dx.doi.org/10.1051/0004-6361:20041664

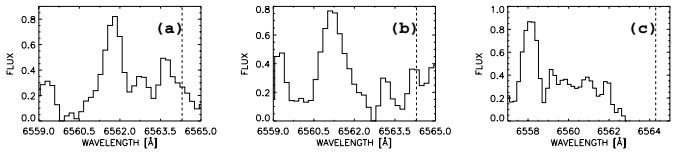


Fig. 6. Fabry-Perot continuum-free spectra of selected regions (see coordinates in Table 3 and white squares in Fig. 1). The spectra are averaged in a box of $8'' \times 8''$ around centres of Table 3. The flux unit is arbitrary. The dashed lines indicate the systemic velocity of the galaxy.

To the West of the field of view, in a region centered at RA $\sim 12^{\rm h}27^{\rm m}39^{\rm s}$, Dec $\sim +13°00'00''$, a very faint and patchy emission is observed at velocities between -80 and 20 km s^{-1}. It is possible that sky emission-line residuals contaminate this extremely low surface brightness region. Nevertheless, most of this emission can be seen in the Kenney & Yale (2002) Hα image, although not discussed, as well as in the Hα image of GoldMine (Gavazzi et al. 2003). Therefore the filamentary structure appears much more complex and extended towards the West than the previously discussed linear filaments.

To the East of F4, a new faint Hα structure is observed, with clumps at velocities between 70–90 km s^{-1} (see e.g. the clump at RA $\sim 12^{\rm h}27^{\rm m}46\overset{\rm s}{.}053$, Dec $\sim +12°59'54\overset{''}{.}06$). These H$\alpha$ clumps superpose on a short X-ray filamentary-like structure in the *Chandra* observations of Machacek et al. (2004), although not discussed by them. The Hα clumps are separated from F4 by a dust lane (see Fig. 7). We think that we do not detect a filament like the X-ray one because our FP profiles are at too low signal-to-noise in this region. For the present time, the origin of the Hα clumps and of the short X-ray structure is unknown: they could have a relation with F4, and/or with the nuclear outflow, or perhaps with the pixels that show a redshifted spectral line in the southern disk region (see previous paragraph).

Three clumps outside the ESO-FP field-of-view have been detected with the OmM observations. Their spectra is shown in Fig. 6 and their velocities listed in Table 3. Their positions are marked by white squares in Fig. 1. The lines observed here cannot be associated to night sky emission-line residuals because these latter always present very sharp wings and are relatively narrower than ionized gas emission-lines, which is not observed. The left panel (Fig. 6a) shows that ionized gas is detected in the SW stellar tail, in the continuity of F3b and with a line at a velocity of $v_{\rm obs} \sim -35$ km s^{-1}. This is comparable with the velocities observed along F3b. On broad-band images, the knot associated with the middle panel spectrum (Fig. 6b) appears as a system having two objects. The right-hand spectrum (Fig. 6c) corresponds to a blue clump on the RGB image of the GoldMine database. These two latter clumps could be HII regions associated with the northern stellar tail. Their velocities appear extremely blue-shifted, in contrast with the kinematics observed in the northern, receding half of the disk. However, because the velocity of any *isolated* clump is known ± 390 km s^{-1} (i.e. the OmM observation free spectral range), it is reasonable to deduce true velocities of $+330$ km s^{-1} and $+190$ km s^{-1} for them, when adding an interfringe to the measured velocities. In this case, their velocities would be in better agreement with the kinematics in the North. Their velocities need to be confirmed by other spectroscopic measurements.

3. Discussion

3.1. Global kinematics of the filaments

Evidence for a high-speed tidal interaction (∼100 Myr ago) with the northern companion NGC 4435 at the origin of the prominent NE and SW stellar tails and of part of the molecular gas above the galactic disk were first presented in Combes et al. (1988). Furthermore, K95 proposed that the off-plane gaseous distribution could be due to an ISM-ISM collision with NGC 4435 and that the gas should be re-accreted into NGC 4438 after the collision.

Numerical simulations of galaxy tidal interactions or mergers (e.g. Hibbard & Mihos 1995; Barnes & Hernquist 1996; Mihos 2001) have shown that most of the material in stellar and gaseous tails remain bound to a parent disk, hence falling back towards it. There are evidence in the velocity field that gas in the filaments is dynamically bound to NGC 4438. Indeed, this study confirms that no extremely high velocity departures with respect to the systemic velocity are observed in the filaments (see also Combes et al. 1988; K95). The highest velocity amplitudes (in absolute values) are found in the disk. Moreover, the filaments seem to participate to the rotation of the galaxy, with redshifted (blue-shifted) gas to the North (South respectively) and with velocities close to the systemic value in parts of F1 and F2 that roughly lie along the minor axis. Though F0 is obviously less redshifted than part of F1 while it is the northernmost filament, this trend exactly follows the disk rotational pattern. The diffuse filaments of NGC 4438 are thus apparently bound to it and it is likely that they will be reaccreted towards the disk.

3.2. Ram pressure stripping

Signatures of ram pressure stripping (hereafter RPS) have already likely been observed in nearby groups and clusters galaxies in the form of linear structures, filaments, off-plane ring-like and comet-like morphologies of either ionized or neutral gas or radio continuum (Gavazzi et al. 2001; Vollmer et al. 2000; Bureau & Carignan 2002; Vollmer et al. 2004a). In the Virgo cluster, there exist observational indications of ongoing or recent RPS. The most probable cases are among the most HI-deficient galaxies, like NGC 4388 (Veilleux et al. 1999; Yoshida et al. 2002; Vollmer & Huchtmeier 2003) or NGC 4522 (Vollmer et al. 2000; Kenney et al. 2004; Vollmer et al. 2004a). A case where a RPS could happen with a gravitational interaction has also been presented for NGC 4654 (Vollmer 2003).

It has been claimed that a tidal interaction and an ISM-ISM collision with NGC 4435 were probably responsible for the displacement of HI and part of the CO gas outside the galaxy plane of NGC 4438 and for the formation of the ionized gas filaments (Combes et al. 1988; K95). NGC 4438 is yet a good candidate for an active RPS by the Virgo ICM (Kotanyi et al. 1983; Cayatte et al. 1990, 1994; K95; Vollmer et al. 2004b). The fact that F2, F3, parts of F0 and F1 and the second half

Article published by EDP Sciences and available at http://www.edpsciences.org/aa or http://dx.doi.org/10.1051/0004-6361:20041664

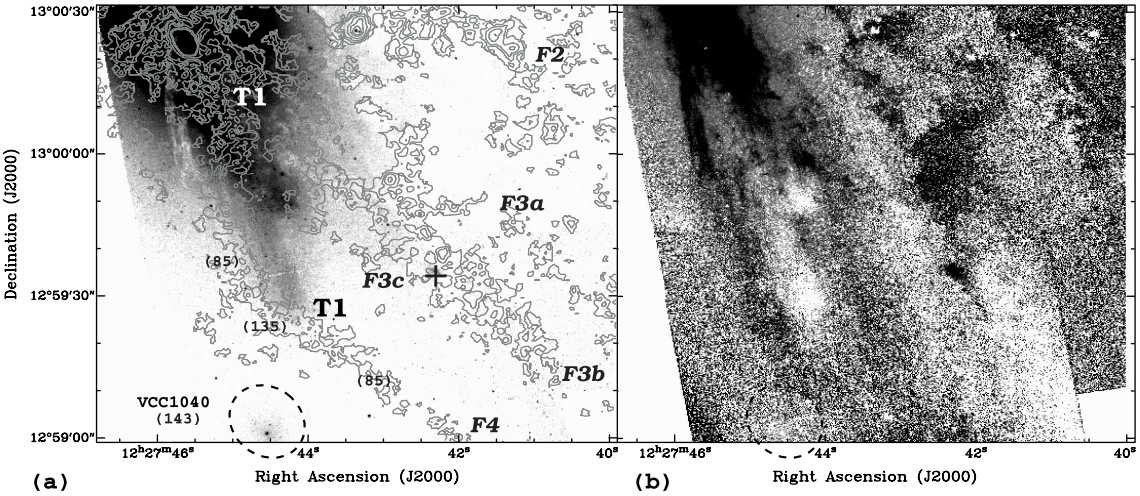


Fig. 7. a) *F450W WFPC2-HST* image showing VCC 1040 and the southern parts of NGC 4438. Full-line contours represent the Hα emission in NGC 4438, a dashed line contour an isophote of VCC 1040. Labels F2 to F4 refer to the Hα filaments. The opposite extremities of the stellar tail T1 are delineated by labels T1. Numbers into brackets represent radial velocities in F4 and of VCC 1040 (in km s^{-1}). A cross marks the location of the object 2MASXiJ1227422+125935 (see text). **b)** *F450W-F814W* colour index map. Dark shades represent dust lanes. The dark area to the East of VCC 1040 is *not* due to dust but to the sky background level.

of F4 are all directed along the NE-SW direction could be an indication that a common stripping process is responsible for their shaping and high degree of collimation.

A key-point for a RPS hypothesis is to explain why no gas is observed at high velocities relative to the galaxy in the Hα filaments. This observational fact is not expected because of the rapid l-o-s relative motion of NGC 4438 with respect to the cluster (~1000 km s^{-1}). If high velocity gas really exists, which reasons could explain its non-detection? Firstly, we recall that our restricted spectral ranges prevent from detecting any extremely high velocity departures w.r.t. the systemic velocity. If present, detecting it would need other observations performed at other wavelengths or with a larger spectral band. However, the Fabry-Perot spatial distribution of Hα matches well the one obtained from deep Hα + [NII] images, showing that no gas is missed by our observation. In other words, it seems implausible that a large amount of gas at high l-o-s velocity exists in the optical filaments. Then, numerical simulations of RPS could help to answer this question. Major improvements on the modelling of RPS have been done recently (Abadi et al. 1999; Quilis et al. 2000; Schulz & Struck 2001; Vollmer et al. 2001) and models succeeded in reproducing kinematical properties and morphological anomalies of cluster galaxies (e.g. Vollmer et al. 2004b). For instance, the case of NGC 4388 is particularly interesting because it is another highly inclined galaxy in the cluster core. A RPS model for NGC 4388 (Vollmer & Huchtmeier 2003) has shown that most of the gas remains bound to the galaxy and that gas particles with the highest velocities w.r.t. the galaxy appear at high distance from the disk (few tens of kpc). The important parameters of such simulations are the ICM density, the galaxy velocity relative to the ICM (2000 km s^{-1} for NGC 4388) and the inclination angle of the galaxy disk to its orbital plane. Although NGC 4438 is orbiting in the Virgo cluster under different conditions than NGC 4388 and could have been considerably disturbed by a massive companion, one could expect that most of its gas resides close the galaxy systemic velocity within the first tens of kpc from the centre, as is observed. If a small fraction of gas with high relative velocity exists, it could be now located further away from the nucleus, outside the field of view. A good test would be to search neutral gas in a very large field-of-view around the galaxy.

Perhaps another good test for an ongoing RPS scenario would be to study the stellar kinematics of the southern region, where filaments F3 and F4 appear to superpose on large and small (respectively) stellar tails. Since RPS only acts on ionized and neutral gas and not on the stars, it is expected that a kinematical decoupling has developed between gas and stars. It should however be remembered here that simulations of galaxy collisions have already shown velocity differences reaching ~50 km s^{-1} between stars and gas in tidal tails (Mihos 2001), though their global evolution remains coupled (re-accretion on the parent galaxy disk, ...). We do not know the amplitude of an hypothetical velocity difference between stars and gas in the concerned regions of NGC 4438 that would be caused by a tidal interaction *alone*. Numerical models of RPS coupled with a tidal interaction should help to disentangle their respective role on the evolution of the filaments.

3.3. A perturbed region to the South

3.3.1. The peculiar Filament F4

Filament F4 is probably the most intriguing observed filament. A *B*-band image taken from the GoldMine database and *F450W*, *F814W WFPC2-Hubble Space Telescope* images taken from the *HST* archive are used to illustrate the tight relation that exists between stars, gas and dust around Filament F4 and the outer southern part of the disk (Figs. 7 to 9). The *WFPC2-HST* images were reduced using the STSDAS package in IRAF. Warm pixels and cosmic ray hits were removed using

Article published by EDP Sciences and available at http://www.edpsciences.org/aa or http://dx.doi.org/10.1051/0004-6361:20041664

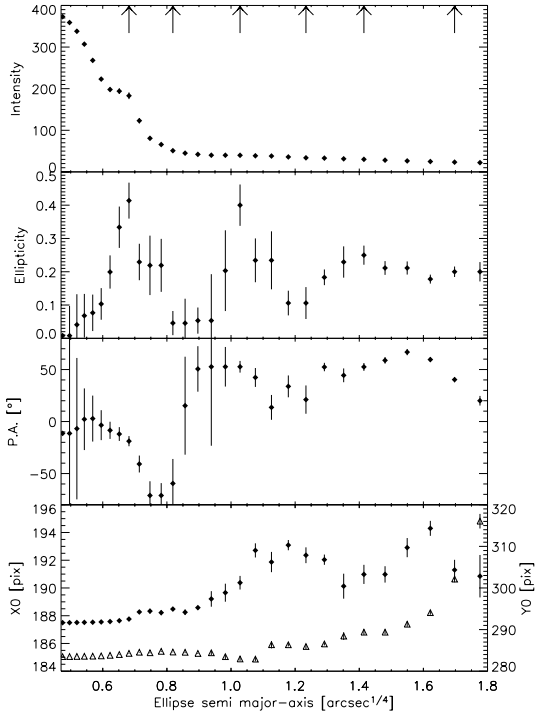


Fig. 8. Isophotal analysis of VCC 1040 from a *F814W WFPC2-HST* image. *From Top to Bottom*: intensity, ellipticity, position angle (in degree), central *X* and *Y* coordinates (in pixel, full dots and open triangles respectively) variations as function of ellipse semi-major axis (in arcsec$^{0.25}$). The arrows indicate the radii of the isophotes displayed in Fig. 9.

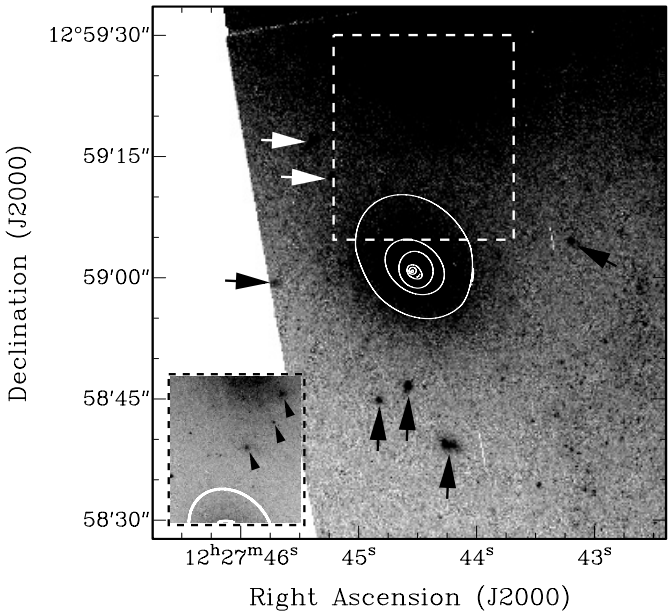


Fig. 9. Enlargement of an *F814W WFPC2-HST* image around VCC 1040. The arrows indicate different clumps surrounding the dwarf galaxy while ellipses indicate fitted isophotes of VCC 1040 to the image at the radii flagged by arrows in Fig. 8. The bottom-left insert is a focus of the white dashed box for another intensity scale to emphasize on brighter clumps *between* the dE and the tip of the stellar tail T1.

the *warmpix* and *crrej* tasks and the final mosaics were created using the *wmosaic* task. Cosmic rays were also treated using the *lacos_im* procedure (van Dokkum 2001). We also built a *F450W-F814W* ($\simeq B - I$) colour index map from the ratio of *F450W* to *F814W* (Fig. 7b) in order to follow the dust lanes and star formation regions across and outside the galactic disk. Basically, redder colours appear here as darker shades and correspond to dusty regions (dust lane associated with the disk and filaments, and the western dust layer) while bluer colours appear as lighter shades and can correspond to star formation sites. The colour index image principally shows that the dust is along a prominent ring-like structure in the inner parts of the galaxy and also present outside the disk to the West and South. HII regions along the filaments have colours as blue as $m_{F450W} - m_{F814W} = -1.3$ mag.

We notice here the presence of an irregular-shaped object with a colour of up to 1.2 mag, lying along the edges of the prominent dust lane and Filament F3b (RA $\sim 12^h27^m42\overset{s}{.}3$, Dec $\sim +12°59'35\overset{''}{.}2$). It is nearly aligned with the bright warped stellar structure of the southern edge of the disk and Filament F3c (Fig. 7a). The only referred object closest to this location is called 2MASXi J1227422+125935 and is classified as a galaxy of diameter 1.′2 in the 2MASS database (Jarrett et al. 2000). We deduce an upper limit "diameter" of ∼6″ from the *F814W-HST* image, which is considerably lower than the referred value. No gas is detected within this object and because its redshift is unknown, it is not yet possible to determine whether it is related to NGC 4438 or whether it is a background galaxy.

As seen in Figs. 7a and 7b, a first half of F4 lies along the eastern edge of a stellar tail (hereafter T1) and exactly superposes on a dust lane. Then F4 bends towards the SE from the tip of T1. The northernmost part of T1 seems to arise from the inner regions of the disk. A lower limit for the length of T1 is 1′ (4.7 kpc). It is shorter than the two large-scale outer tails, which extend on distances of at least 4.′1 (or 19 kpc) towards the NE and 3.′1 (or 14.5 kpc) towards the SW. T1 is obviously crossed by a brighter and warped stellar tail (RA $\sim 12^h27^m44.5^s$, Dec $\sim +12°59'55''$, Fig. 7a). Figure 7a shows that this bright warped stellar tail arises from the SE near side of the galaxy disk. T1 then lies straight towards the South, pointing in the direction of VCC 1040, a dwarf elliptical galaxy. It has a lower surface brightness than the stellar disk and the bulge/halo of NGC 4438. The tips of T1 and the brighter warped tail have blue colours (−0.2 mag. on average). T1 is reminiscent of tidal stellar streams like those observed around massive spirals such as the Milky Way (Ibata et al. 2001a) or Messier 31 (Ibata et al. 2001b). The next section presents arguments to explain its formation by the presence of VCC 1040.

3.3.2. A role for VCC 1040?

VCC 1040 is a dwarf-nucleated elliptical galaxy and is the closest companion of NGC 4438. It is projected at only 1.′5 (7 kpc) from the nucleus of NGC 4438 (to be compared with 4.′5 or 21 kpc between NGC 4435 and NGC 4438) and ∼25″ (2 kpc) from F4. It has a redshift of -143 ± 63 km s^{-1} (Conselice et al. 2001) which coincides within the errors with the velocity of the region where F4 bends and with the mean radial velocity of F4. Though dwarf elliptical galaxies are the

Article published by EDP Sciences and available at http://www.edpsciences.org/aa or http://dx.doi.org/10.1051/0004-6361:20041664

most common type of galaxies found in the local galaxy clusters like Virgo (Ferguson & Binggeli 1994) and the probability of finding foreground or background dEs in the direction of the cluster core is high, their proximity in sky position and redshift likely makes VCC 1040 a genuine companion of NGC 4438. Its colour index $B-R$ is 1.6 (K95) and indicates an old object (i.e. with an age $\gg$ 100 Myr), which is usual for dEs (Rakos et al. 2001; Conselice et al. 2003; Jerjen et al. 2004), and no ionized gas is found in it.

K95 have noticed the presence of several apparent stellar clump debris including VCC 1040, which could have been formed during the interaction between NGC 4435 and NGC 4438. Tidal dwarf galaxy candidates are usually blue, gas rich, young and irregular-typed structures always observed along stellar tidal tails (e.g. Duc et al. 1997), which properties do not match with those of VCC 1040. Morever the time-scale invoked to form a dE is several hundred Myr (Kroupa 1998), which is shorter than the elapsed time since the interaction between NGC 4435 and NGC 4438 (~100 Myr according to the Combes et al.' simulations). It seems unlikely for VCC 1040 to be a tidal dwarf galaxy.

Several elements show that the environment around VCC 1040 and VCC 1040 itself are perturbed. Firstly, an Hα emission is found between Filament F4 and the dwarf galaxy (Fig. 7a). This emission actually appears to be an unusual ionized gas loop to the East of the F4 bending region.

Secondly, the isophotal analysis of the dE light distribution reveals its perturbed morphology, as shown in Figs. 8 and 9. Ellipses of variable geometrical parameters (centre coordinates $X0$ and $Y0$, ellipticity and position angle of the isophotes) were fitted to a *F814W WFPC2-HST* image. A lower limit of the VCC 1040 radius is thus ~10″ (780 pc), i.e. for the last accurately measured isophote. K95 found an outer radius of 14″. At higher radius than 10″, the light distribution is partly contaminated by the diffuse stellar light of NGC 4438 and by dust to the N and NW outer parts of the dE, hence results are not shown for these radii due to too large uncertainties on the parameters. The graphs show that there is a substantial offset of the position of the photometrical centre as the radius increases and that the Y-offset of the outer ellipses is larger than the X-offset. As an example, the isophote with semi-major axis $r \sim 8\farcs4$ (last arrow) has its centre offset by ~1.″8 (140 pc) to the N-NW direction with respect to the innermost isophotes, within a ratio of $\frac{Y-\text{offset}}{X-\text{offset}} = 6$. Moreover, the galaxy is less rounder in its outer parts ($\epsilon \rightarrow 0.2$) than in its inner ones ($\epsilon \sim 0.05$ for $0\farcs4 \leq r \leq 1''$), though passing through a significant peak at $r = 1\farcs1$ ($\epsilon = 0.4$). Twists of the isophotes are also clearly detected. The PA indeed drastically varies between ~10° and 70° (for $r > 0.5''$). At a radius of ~0.″25, the intensity bump, the ellipticity peak and the drastic change of photometric PA are likely due to the nucleus of the dwarf. Figure 9 displays some isophotal ellipses (which semi-major axis positions are flagged by arrows in Fig. 8) and illustrates well the measured asymmetry of the dE.

Finally, numerous clumps are observed in the close vicinity of VCC 1040 as well as between the dwarf galaxy and the tip of T1 (Fig. 9). Their colour range is large, from blue to red clumps (−1 to 2 mag) indicating that they could be gas rich objects to old globular clusters. No gas was detected in them and their radial velocities are unknown so that their possible association with the southern region remains to be confirmed. Other knotty structures are found within the NE and SW large-scale stellar tidal arms (K95). It is surprising to find stellar clumps all around the dE, because they are not directly associated to the large-scale tails. Potential reservoir of stars for them could thus be VCC 1040 or T1.

Which mechanism could explain all these perturbations? We emphasize here on a minor tidal interaction event that could have occurred (or perhaps that would be occuring) between VCC 1040 and NGC 4438, due to the presence of the dust lane and of the stellar tail (T1) both pointing towards VCC 1040 and to the fact that the VCC 1040 redshift is comparable with velocities observed along the gaseous Filament F4, and thus perhaps with the velocity of the tail. A comparison of the VCC 1040 tidal radius $r_{\rm t} = R\left(\frac{m}{3M}\right)^{\frac{1}{3}} \sim 7''$ (0.5 kpc) with the VCC 1040 radius of $r \gtrsim 10''$ (0.78 kpc) implies that a tidal stripping of its external parts by the gravitational forces of NGC 4438 could be ongoing. We have used here $R \sim 7$ kpc as the distance between the two galaxies, $m \propto 10^8\ M_\odot$ as the mass of VCC 1040, which is typical of dwarf ellipticals, $M \propto 10^{11}\ M_\odot$ for NGC 4438 (Combes et al. 1988)[2]. Early simulations of the encounter with NGC 4435 (Combes et al. 1988) did not predict T1 but only the large-scale stellar asymmetry of NGC 4438 and one has to imagine another triggering event for its formation. The stream T1 and the stellar concentrations around the dwarf galaxy can be consequences of such a minor tidal event. Photometrical anomalies are often observed in dwarf early-type galaxies of the Virgo cluster (Binggeli et al. 2000; Barazza et al. 2003) and it is still unclear whether they are due to intrinsic or external perturbations to the dwarf galaxies. We think that the asymmetries measured in VCC 1040 are of the same nature as those measured in other dEs. An interaction with NGC 4438 could also explain the photometrical disturbance of VCC 1040, by stretching the outer parts towards NGC 4438, as measured from the isophotal analysis.

This would not be the first time that a minor interaction opposing two galaxies, one large and one dwarf, is observed in the Virgo cluster. Other possible cases have indeed been presented with the couples M49-VCC 1249 (Sancisi et al. 1987; McNamara et al. 1994), NGC 4694-VCC 2062 (van Driel & van Woerden 1989; Hoffman et al. 1993) and M 86-VCC 882 (Elmegreen et al. 2000). A detailed analysis of the stellar populations in the tails and in the galaxies would be very useful to test the minor interaction hypothesis.

4. Conclusions

New optical observations in the Hα emission-line of the Virgo cluster galaxy NGC 4438 were presented, as part of a large survey dedicated to the kinematics of Virgo spiral galaxies. Using Fabry-Perot interferometry data at an effective angular resolution of ~2″, the optical velocity field of the galaxy was mapped

[2] The estimated value of the tidal radius is a lower limit because of the use of the *projected* distance of the dwarf to the nucleus of NGC 4438.

Article published by EDP Sciences and available at http://www.edpsciences.org/aa or http://dx.doi.org/10.1051/0004-6361:20041664

for the first time. NGC 4438 is one of the most disturbed Virgo spirals which has probably undergone a tidal interaction with the massive companion NGC 4435, and which is probably undergoing the effects of ram pressure stripping by the hot ICM in the cluster core. The Hα velocity field reveals the complex gas kinematics within the galactic disk, the nuclear shells and the external filaments. Our conclusions can be summarized as follows:

(1) The nuclear shell of NGC 4438 is likely expanding, as revealed by the multiple spectral components detected in the FP data-cube along the NW shell. Further observations of the nuclear region at higher spectral resolution and larger spectral coverage than our observations are needed to investigate the internal motions of the nuclear outflow.
(2) A new filament is observed to the North of the disk. It is short, clumpy and has no X-ray counterparts while the other filaments are much more extended, diffuse and exhibit a X-ray counterpart. Two velocity components are observed in some pixels of the data-cube in the approaching side of the disk. One of the component has a redshifted kinematics which totally contrasts with the local, blueshifted velocity field of the approaching half. Its velocity is however consistent with that found in nearby, diffuse, off-plane knots, suggesting that both could belong to a same morphological structure. The global kinematics of the extended filaments indicate that they are likely bound to the galaxy.
(3) A tight relation between the presence of a small stellar tail aligned with a dust lane and an Hα filament South of the galaxy, and of the dwarf elliptical galaxy VCC 1040 is outlined. The gaseous filament suddenly changes its orientation at the tip of the stellar stream. The VCC 1040 redshift is comparable with velocities observed in the Hα filament. We suggest that a minor tidal interaction has occurred, or is perhaps occurring, between NGC 4438 and the dwarf galaxy, causing the disruption of the small galaxy and the formation of the stellar tail.

Further 3D numerical simulations taking into account both tidal interactions and ram pressure stripping would be crucial to improve our understanding of the evolution of this complex system.

Acknowledgements. We thank Marie Machacek for gratefully providing with the *Chandra* X-ray image of the galaxy and for interesting discussions, Anthony Moffat for a careful reading of the manuscript, Olivier Daigle for his technical support and the anonymous referee for constructive remarks. This work was partly funded by the grant Regroupement Stratégique – Observatoire du Mont Mégantic of FQRNT (Québec) and by the Ministère de l'Éducation Nationale, de la Recherche et de la Technologie (France). We made use of GoldMine – Galaxy On Line Database Milano Network (`http://goldmine.mib.infn.it`) and the *Hubble Space Telescope* data archive (`http://archive.stsci.edu/hst`).

References

Abadi, M. G., Moore, B., & Bower, R. 1999, MNRAS, 308, 947
Barazza, F. D., Binggeli, B., & Jerjen, H. 2003, A&A, 407, 121
Barnes, J. E., & Hernquist, L. 1996, ApJ, 471, 115
Binggeli, B., Sandage, A., & Tammann, G. A. 1985, AJ, 90, 1681
Binggeli, B., Barazza, F., & Jerjen, H. 2000, A&A, 359, 447
Bureau, M., & Carignan, C. 2002, AJ, 123, 1316
Cayatte, V., van Gorkom, J. H., Balkowski, C., et al. 1990, AJ, 100, 604
Cayatte, V., Kotanyi, C., Balkowski, C., et al. 1994, AJ, 107, 1003
Chemin, L., Cayatte, V., Balkowski, C., et al. 2003, A&A, 405, 89
Chemin, L., Balkowski, C., Cayatte, V., et al. 2004, in SF2A 2004, ed. F. Combes, D. Barret, T. Contini, F. Meynadier, & L. Pagani (EDP Sciences) [arXiv:astro-ph/0410308]
Combes, F., Dupraz, C., Casoli, F., et al. 1988, A&A, 203, L9
Conselice, C. J., Gallagher, J. S., & Wyse, R. F. G. 2001, ApJ, 559, 791
Conselice, C. J., Gallagher, J. S., & Wyse, R. F. G. 2003, AJ, 125, 66
Duc, P.-A., Brinks, E., Wink, J. E., et al. 1997, A&A, 326, 537
Elmegreen, D. M., Elmegreen, B. G., Chromey, F. R., et al. 2000, AJ, 120, 733
Ferguson, H. C., & Binggeli, B. 1994, A&AR, 6, 67
Gach, J.-L., Hernandez, O., Boulesteix, J., et al. 2002, PASP, 114, 1043
Gavazzi, G., Boselli, A., Mayer, L., et al. 2001, ApJ, 563, L23
Gavazzi, G., Boselli, A., Donati, A., et al. 2003, A&A, 400, 451
Gnedin, O. Y. 2003, ApJ, 589, 752
Gooch, R. E. 1995, in Astronomical Data Analysis Software and Systems IV, ed. R. A. Shaw, H. E. Payne, & J. J. E. Hayes (San Francisco: ASP), ASP Conf. Ser., 77, 144
Gunn, J. E., & Gott, J. R. 1972, ApJ, 176, 1
Hibbard, J. E., & Mihos, J. C. 1995, AJ, 110, 140
Ho, L. C., Filippenko, A. V., & Sargent, W. L. W. 1997, ApJS, 112, 351
Hoffman, G. L., Lu, N. Y., Salpeter, E. E., et al. 1993, AJ, 106, 39
Hummel, E., van Gorkom, J. H., & Kotanyi, C. 1983, ApJ, 267, L5
Ibata, R., Lewis, G. F., Irwin, M., et al. 2001a, ApJ, 551, 294
Ibata, R., Irwin, M., Lewis, G. F., et al. 2001b, Nature, 412, 49
Jarrett, T. H., Chester, T., Cutri, R., et al. 2000, AJ, 119, 2498
Jerjen, H., Binggeli, B., & Barazza, F. D. 2004, AJ, 127, 771
Keel, W. C., & Wehrle, A. E. 1993, AJ, 106, 236
Kenney, J. D. P., Rubin, V. C., Planesas, P., et al. 1995, ApJ, 438, 135 [K95]
Kenney, J. D. P., & Yale, E. E. 2002, ApJ, 567, 865
Kenney, J. D. P., van Gorkom, J. H., & Vollmer, B. 2004, AJ, 127, 3361
Kotanyi, C., van Gorkom, J. H., & Ekers, R. D. 1983, ApJ, 273, L7
Kroupa, P. 1998, MNRAS, 300, 200
Machacek, M. E., Jones, C., & Forman, W. R. 2004, ApJ, 610, 183
McNamara, B. R., Sancisi, R., Henning, P. A., et al. 1994, AJ, 108, 844
Mihos, J. C. 2001, ApJ, 550, 94
Moore, B., Katz, N., Lake, G., et al. 1996, Nature, 379, 613
Quilis, V., Moore, B., & Bower, R. 2000, Science, 288, 1617
Rakos, K., Schombert, J., Maitzen, H. M., et al. 2001, AJ, 121, 1974
Schulz, S., & Struck, C. 2001, MNRAS, 328, 185
Sancisi, R., Thonnard, N., & Ekers, R. D. 1987, ApJ, 315, L39
van Dokkum, P. G. 2001, PASP, 113, 1420
van Driel, W., & van Woerden, H. 1989, A&A, 225, 317
Veilleux, S., Cecil, G., Bland-Hawthorn, J., et al. 1994, ApJ, 433, 48
Veilleux, S., Bland-Hawthorn, J., Cecil, G., et al. 1999, ApJ, 520, 111
Vollmer, B. 2003, A&A, 398, 525
Vollmer, B., & Huchtmeier, W. 2003, A&A, 406, 427
Vollmer, B., Marcelin, M., Amram, P., et al. 2000, A&A, 364, 532
Vollmer, B., Cayatte, V., Balkowski, C., et al. 2001, ApJ, 561, 708
Vollmer, B., Beck, R., Kenney, J. D. P., et al. 2004a, AJ, 127, 3375
Vollmer, B., Balkowski, C., Cayatte, V., et al. 2004b, A&A, 419, 35
Yoshida, M., Yagi, M., Okamura, S., et al. 2002, ApJ, 567, 118

Article published by EDP Sciences and available at http://www.edpsciences.org/aa or http://dx.doi.org/10.1051/0004-6361:20041664